Wireless Power Transfer With Zero-Phase-Difference Capacitance Control

Shunta Iguchi, *Student Member, IEEE*, Pyungwoo Yeon, *Student Member, IEEE*, Hiroshi Fuketa, *Member, IEEE*, Koichi Ishida, *Member, IEEE*, Takayasu Sakurai, *Fellow, IEEE*, and Makoto Takamiya, *Senior Member, IEEE*

***Abstract*—Wireless power transfer enables the frequent and ubiquitous charging of electronic devices. However, the variation of the efficiency and the received power with the transmission distance is an outstanding issue. To solve the problem of efficiency degradation of the magnetic resonance at short distances, zero-phase-difference capacitance control (ZPDCC), which is suitable for integration in large scale integrations (LSIs) is proposed in this paper. The proposed ZPDCC achieves adaptive capacitance control by a newly proposed control algorithm with a current-sensing circuit to control variable capacitors at a fixed frequency. Additionally, a theoretical analysis of the total DC-DC power transmission efficiency ($\eta_{\rm TOTAL}$) including a power amplifier, coupled resonators, and a rectifier is demonstrated in this paper. The analysis indicates that the frequency (and capacitance) splitting of $\eta_{\rm TOTAL}$ is mainly due to the power amplifier; additionally, the efficiency of the power amplifier is maximized at the split peaks when the transmission distance (d) is short. A wireless power transfer system in magnetic resonance with ZPDCC is fabricated in a 3.3 V, 180 nm CMOS. By introducing ZPDCC, the measured $\eta_{\rm TOTAL}$ at 13.56 MHz increases 1.7 times from 16% to 27% at $d = 2.5$ mm.**

***Index Terms*—Magnetic resonance, power amplifier, wireless power transmission, zero-phase-difference capacitance control.**

I. Introduction

Wireless power transfer has opened a new era of power distribution without messy wire connections and the inconvenience of charging batteries. Wireless power transfer enables the frequent and ubiquitous charging of electronic devices (e.g., cell phones). However, the transmission efficiency is degraded by radiation loss and the resistive loss of antennas; additionally, the variation of the efficiency and the received power with the transmission distance is also an outstanding issue.

As first proposed in 2007 [1], magnetic resonance has the potential to realize more efficient and stable wireless charging at intermediate distances (1 cm–10 m) than a conventional microwave beam [2] and magnetic induction [3]. Wireless power transmission systems with magnetic resonance consist of a power amplifier, coupled resonators, and a rectifier. The total DC-DC power transmission efficiency ($\eta_{\rm TOTAL}$) at the inherent resonant frequency ($f_{\rm RES}$) of the resonators is maximized at a certain distance, while $\eta_{\rm TOTAL}$ is reduced at short distances (e.g., 1 cm). This efficiency degradation at short distances is a unique phenomenon of magnetic resonance and is not observed in conventional magnetic induction.

To address this issue, several techniques [4]–[20] and theoretical studies [21]–[23] have been reported. Frequency tracking [4]–[9] controls the transmission frequency corresponding to the transmission distance, although frequency deviation is not allowed in many radio bands (e.g., the ISM band [24]). A repeater coil array [10], [11] has a misalignment-tolerant design without frequency deviation; however, the number of transmission coils has to be increased to cover a large misalignment. This increases the size and cost of the transmitter. Supply voltage ($V_{\rm DD}$) control [12], [13] controls the output power of a power amplifier to regulate the received power, although $\eta_{\rm TOTAL}$ is greatly reduced by the loss of the DC-DC converter. To address this degradation of efficiency, adaptive impedance matching [14]–[18] has been introduced. The optimum load impedance of a power amplifier has been realized using variable capacitors [15]–[18], while in several studies, a bulky and expensive directional coupler [14], [15] and impedance analyzer [16], [17] were required as detectors.

A theoretical analysis of $\eta_{\rm TOTAL}$ including a power amplifier, coupled resonators, and a rectifier is newly demonstrated in this paper. The results indicate that the frequency (and capacitance) splitting of $\eta_{\rm TOTAL}$ is mainly due to the power amplifier and that the efficiency at short distances is maximized at the split peaks. This verifies the effect of zero-phase-difference capacitance control (ZPDCC) [19]. The proposed ZPDCC is suitable for integration in large scale integrations (LSIs) to reduce efficiency degradation of the magnetic resonance at short distances. The proposed ZPDCC achieves adaptive capacitance control by a newly proposed control algorithm with a current-sensing circuit to control variable capacitors at a fixed frequency.

An outline of this paper is given as follows. In Section II, a theoretical analysis of the efficiency degradation of the magnetic resonance at short distances is given. In Section III, a method that increases $\eta_{\rm TOTAL}$ at short distances without frequency deviation and the need for a bulky detector circuit is proposed. In Section IV, the measured results for a wireless power transfer circuit with ZPDCC are reported. In Section V, conclusions are given.

II. Analysis of Efficiency of Magnetic Resonance

In this section, a theoretical analysis of the efficiency degradation of the magnetic resonance at short distances is given, in particular, the frequency dependence of the efficiency of coupled resonators ($\eta_{\rm RES}$) and a power amplifier ($\eta_{\rm PA}$) is clarified by theoretical calculations and simulations. These calculations and simulations indicate that frequency splitting is not observed

Manuscript received August 31, 2014; revised December 11, 2014; accepted December 23, 2014. Date of current version March 27, 2015. This work was supported in part by Renesas Electronics Corporation. This paper was recommended by Associate Editor R. Gomez-Garcia.

S. Iguchi, H. Fuketa, T. Sakurai, and M. Takamiya are with the University of Tokyo, Tokyo 153-8505, Japan (e-mail: shiguchi@iis.u-tokyo.ac.jp).

P. Yeon was with the University of Tokyo, Tokyo 153-8505, Japan. He is now with Georgia Institute of Technology, Atlanta, GA 30308 USA.

K. Ishida was with the University of Tokyo, Tokyo 153-8505, Japan. He is now with Technische Universität Dresden, Dresden 01069, Germany.

Color versions of one or more of the figures in this paper are available online at http://ieeexplore.ieee.org.

Digital Object Identifier 10.1109/TCSI.2015.2388832

in $\eta_{\rm RES}$ with asymmetric port impedances, while it is observed in $\eta_{\rm PA}$. Several studies [4], [7], [15], [16] have investigated the increase in the efficiency between coupled resonators with port impedances of 50 Ω. The efficiency is calculated from $|S_{21}|^2$ measured by a vector network analyzer. However, these studies gave limited conclusions because not only coupled resonators but also a power amplifier made a large contribution to $\eta_{\rm TOTAL}$. This study includes a new theoretical analysis of $\eta_{\rm TOTAL}$ and frequency splitting while taking into account the effect of $\eta_{\rm PA}$. In this section, the frequency dependence of $\eta_{\rm TOTAL}$ with a power amplifier, coupled resonators, and a rectifier is theoretically analyzed to clarify the effect of a power amplifier.

A. Transmission Efficiency Between Coupled Resonators

To analyze the efficiency degradation at short distances and discuss the frequency splitting in the case of asymmetric port impedances, the frequency dependence of $\eta_{\rm RES}$ is first analyzed. Figs. 1(a) and (b) show a schematic of a wireless power transfer system and the equivalent circuit in magnetic resonance with a power amplifier, coupled resonators, and a rectifier, respectively. $V_{\rm DD}$ is the supply voltage of the power amplifier, $L_{\rm RES}$ is the inductor in each resonator, $C_{\rm RES}$ is the capacitor in each resonator, $C_{\rm L}$ is the load capacitor at the output of the rectifier, $R_{\rm L}$ is a load resistor at the output of the rectifier, k is the coupling coefficient of the coupled resonators, $R_{\rm RES}$ is the equivalent series resistor of the $L_{\rm RES}$, $L_{\rm M}$ is the mutual inductor corresponding to $kL_{\rm RES}$, $V_{\rm IN}$ is the output voltage of the power amplifier, $I_{\rm IN}$ is the output current of the power amplifier, $R_{\rm IN(RECT)}$ is the input resistor of the rectifier, and $Z_{\rm IN}$ is the input impedance of the coupled resonators. Additionally, the input power to the power amplifier, the output power of the power amplifier, the input power to the rectifier, and the load power are denoted as P_1, P_2, P_3, and P_4, respectively. Then, the efficiency of the power amplifier, coupled resonators, and rectifier, and the total DC-DC power transmission are respectively defined as

$$\eta_{\rm PA} = \frac{P_2}{P_1} \tag{1}$$

$$\eta_{\rm RES} = \frac{P_3}{P_2} \tag{2}$$

$$\eta_{\rm RECT} = \frac{P_4}{P_3} \tag{3}$$

$$\eta_{\rm TOTAL} = \eta_{\rm PA} \times \eta_{\rm RES} \times \eta_{\rm RECT} = \frac{P_4}{P_1}. \tag{4}$$

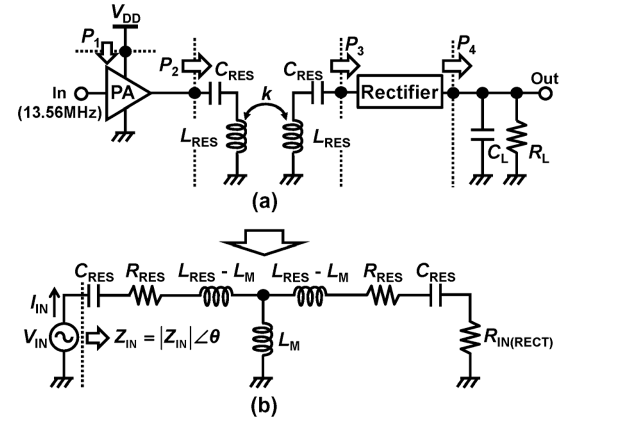

Fig. 1. Schematic of a wireless power transfer system. (a) Block diagram of system with a power amplifier, coupled resonators, and a rectifier. (b) Equivalent circuit.

In previous studies [4], [7], [10], [14]–[17], [23] with a port impedance of 50 Ω, $\eta_{\rm RES}$ was defined by $|S_{21}|^2$. Integrated wireless power transfer systems are implemented using a digital power amplifier (e.g., class-D [8], [9], [19] or class-E [12], [13], [18], [20]) to maximize $\eta_{\rm PA}$ and $\eta_{\rm TOTAL}$. The output impedance corresponding to the on-resistance of a power transistor is lower than 50 Ω; additionally, the input impedance of a rectifier varies with the load resistance $(R_{\rm L})$. Therefore, the port impedances of the coupled resonators are not symmetric. A previous theoretical study [21] showed that the frequency splitting of $\eta_{\rm RES}$ is not observed in the case of asymmetric port impedances, while it is observed in the case of symmetric port impedances. This conclusion was obtained by differential calculations of $1/\eta_{\rm RES}$ as shown in [21]. To support the discussions of $\eta_{\rm PA}$ in the next section, a discussion and findings regarding $\eta_{\rm RES}$ in the case of asymmetric port impedances are given in this section.

It is first assumed that the coupled resonators of the transmitter and receiver are configured by the same components and that the output impedance of the power amplifier is negligible, compared with the input impedance of the rectifier. Then, $\eta_{\rm RES}$ in Fig. 1(b) is given by (5), where the Q is the Q factor of the $L_{\rm RES}$, ω is the angular carrier frequency, and ω_0 is the resonant angular frequency of the $L_{\rm RES}$ and $C_{\rm RES}$. By differentiating (5) with respect to ω, the angular frequency $(\omega_{\eta\,\max})$ at the maximum $\eta_{\rm RES}$ is given by (6). $\eta_{\rm RES}$ has a maximum value at $\omega_{\eta\,\max}$, and which means that $\eta_{\rm RES}$ in the case of asymmetric port impedances does not show frequency splitting. Under the condition $\omega = \omega_{\eta\,\max}$, the maximum $\eta_{\rm RES}$ $(\eta_{\rm RESMAX})$ is given

$$\eta_{\rm RES} = \frac{k^2 L_{\rm RES} Q^3 R_{\rm IN(RECT)} \omega^4}{k^2 L_{\rm RES} Q^2 \omega^4 \left(Q R_{\rm IN(RECT)} + L_{\rm RES}\omega_0\right) + \omega_0 \left[2 L_{\rm RES} Q R_{\rm IN(RECT)} \omega^2 \omega_0 + L_{\rm RES}^2 \omega^2 \omega_0^2 + Q^2 \left\{R_{\rm IN(RECT)}^2 \omega^2 + L_{\rm RES}^2 \left(\omega^2 - \omega_0^2\right)^2\right\}\right]} \tag{5}$$

$$\omega_{\eta\,\max} = \frac{\sqrt{2} L_{\rm RES} Q \omega_0^2}{\sqrt{-Q^2 R_{\rm IN(RECT)}^2 - 2 L_{\rm RES} Q R_{\rm IN(RECT)} \omega_0 + L_{\rm RES}^2 (-1 + 2Q^2) \omega_0^2}} \tag{6}$$

$$\eta_{\rm RESMAX} = \frac{4k^2 L_{\rm RES}^3 Q^5 R_{\rm IN(RECT)} \omega_0^3 / \left(Q R_{\rm IN(RECT)} + L_{\rm RES}\omega_0\right)}{-Q^3 R_{\rm IN(RECT)}^3 - 3 L_{\rm RES} Q^2 R_{\rm IN(RECT)}^2 \omega_0 + L_{\rm RES}^2 Q (-3 + 4Q^2) R_{\rm IN(RECT)} \omega_0^2 + L_{\rm RES}^3 (-1 + 4Q^2 + 4k^2 Q^4) \omega_0^3} \tag{7}$$

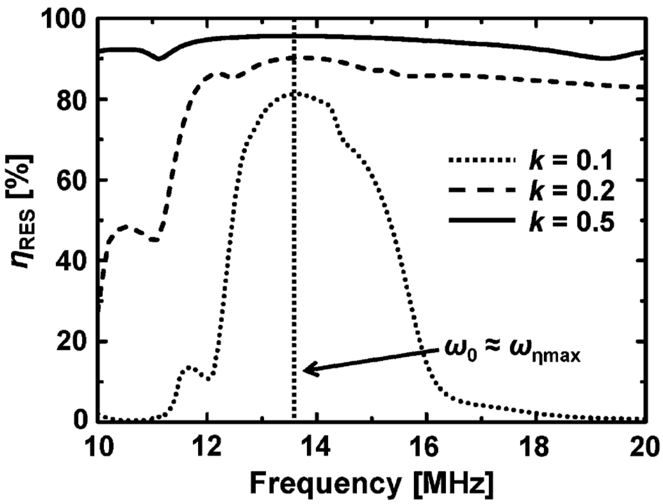

Fig. 2. Simulated frequency dependences of η_{RES} for $k = 0.1$, 0.2, and 0.5 with the parameters in Table I. The simulations include a power amplifier, coupled resonators, and a rectifier as shown in Fig. 1(a). The simulated frequency dependences of η_{RES} do not show frequency splitting even with the nonlinearity induced by the power amplifier and rectifier.

TABLE I
PARAMETERS IN SIMULATIONS

L_{RES}	C_{RES}	Q (L_{RES})	C_{L}	R_{L}	V_{DD}
3.3μH	42pF	100	1μF	80Ω	3.3V

by (7) (see equations at bottom of next page). η_{RESMAX} is a monotonically increasing function of k because the derivative of (7) with respect to k is positive for all k excluding $k = 0$. These results indicate that η_{RES} increases inversely proportionally to the transmission distance without frequency splitting when the port impedances are asymmetric.

Fig. 2 and Table I show the simulated frequency dependences of η_{RES} and the parameters used in the simulations, respectively. The parameters in Table I are determined to achieve $P_4 = 50$ mW at a transmission distance and carrier frequency of 30 mm and 13.56 MHz, respectively. The frequency dependences of η_{RES} in Fig. 2 were simulated by SPICE simulation [25] including a power amplifier, coupled resonators, and a rectifier as shown in Fig. 1(a). The simulated result for η_{RES} demonstrates that η_{RES} is maximized at $\omega \approx \omega_0$ and increases with k. This result is consistent with the conclusion that η_{RES} increases inversely proportionally to the transmission distance without frequency splitting. It should be noted that $\omega_{\eta\max}$ is approximately equal to ω_0 when $R_{\mathrm{IN(RECT)}}$ is small (e.g., less than 100 Ω under the conditions in Table I), while $\omega_{\eta\max}$ increases when $R_{\mathrm{IN(RECT)}}$ is large. In this study, the deviation of $\omega_{\eta\max}$ is negligible because $R_{\mathrm{IN(RECT)}}$ is small.

B. *Frequency Dependence of* η_{PA}

The efficiency of the power amplifier is of fundamental importance in a wireless power transfer system because the frequency splitting of η_{TOTAL} is attributed to η_{PA}. Figs. 3(a) and (b) show the Z_{IN} dependences of the output power (P_2) and drain efficiency (η_{PA}) of a power amplifier obtained by a load pull simulation, respectively. P_2 and η_{PA} are fundamentally determined by Z_{IN}. The simulated results show that P_2 and η_{PA}

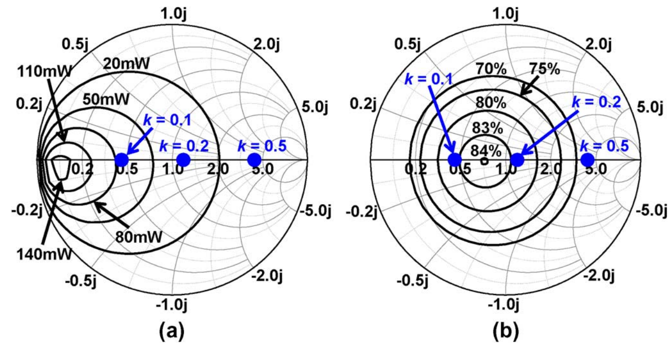

Fig. 3. Z_{IN} dependences of (a) P_2 and (b) η_{PA} for a power amplifier obtained by load pull simulation at 13.56 MHz. Blue dots show the impedances of Z_{IN} for $k = 0.1$, 0.2, and 0.5 with coupled resonators and a rectifier.

increase when $\mathrm{Re}[Z_{\mathrm{IN}}]$ is decreased and $\mathrm{Im}[Z_{\mathrm{IN}}] = 0$. However, $\mathrm{Re}[Z_{\mathrm{IN}}]$ increases proportionally to k; therefore, P_2 and η_{PA} decrease with increasing k.

To clarify the frequency dependence of the η_{PA}, the frequency dependence of Z_{IN} is theoretically analyzed from the equivalent circuit in Fig. 1(b).

First, Z_{IN} is given by

$$Z_{\mathrm{IN}} = \frac{\omega R_{\mathrm{IN(RECT)}} + jL_{\mathrm{RES}}\left\{\left(\omega^2-\omega_0^2\right) - \frac{k^2\omega^4}{\left(\omega^2-\omega_0^2\right)}\right\}}{\omega\left(1 - j\frac{R_{\mathrm{IN(RECT)}}\omega}{\left(\omega^2-\omega_0^2\right)L_{\mathrm{RES}}}\right)} \tag{8}$$

assuming that $R_{\mathrm{RES}} = 0$ for conciseness. Then, $\mathrm{Re}[Z_{\mathrm{IN}}]$ and $\mathrm{Im}[Z_{\mathrm{IN}}]$ are respectively given by

$$\mathrm{Re}[Z_{\mathrm{IN}}] = \frac{k^2L_{\mathrm{RES}}^2R_{\mathrm{IN(RECT)}}\omega^4}{R_{\mathrm{IN(RECT)}}^2\omega^2 + L_{\mathrm{RES}}^2\left(\omega^2-\omega_0^2\right)^2} \tag{9}$$

$$\mathrm{Im}[Z_{\mathrm{IN}}] = \frac{R_{\mathrm{IN(RECT)}}^2\omega^2 + L_{\mathrm{RES}}^2\left\{\left(\omega^2-\omega_0^2\right)^2 - k^2\omega^4\right\}}{\frac{R_{\mathrm{IN(RECT)}}^2\omega^3}{L_{\mathrm{RES}}\left(\omega^2-\omega_0^2\right)} + L_{\mathrm{RES}}\omega\left(\omega^2-\omega_0^2\right)}. \tag{10}$$

Equation (9) shows that $\mathrm{Re}[Z_{\mathrm{IN}}]$ is maximized at $\omega = \omega_0$ and increases proportionally to k^2. This k dependence of $\mathrm{Re}[Z_{\mathrm{IN}}]$ is also verified in Fig. 3.

To increase P_2 and η_{PA}, the condition $\mathrm{Im}[Z_{\mathrm{IN}}] = 0$ should be satisfied. When $\mathrm{Im}[Z_{\mathrm{IN}}] = 0$, ω is given by

$$\omega_{\mathrm{LOW}} = \sqrt{\frac{1 + \sqrt{1 + \frac{4(-1+k^2)L_{\mathrm{RES}}^4\omega_0^4}{\left(R_{\mathrm{IN(RECT)}}^2 - 2L_{\mathrm{RES}}^2\omega_0^2\right)^2}}}{\frac{2(-1+k^2)L_{\mathrm{RES}}^2}{R_{\mathrm{IN(RECT)}}^2 - 2L_{\mathrm{RES}}^2\omega_0^2}}}, \tag{11}$$

$$\omega_{\mathrm{CENTER}} = \omega_0, \tag{12}$$

$$\omega_{\mathrm{HIGH}} = \sqrt{\frac{1 - \sqrt{1 + \frac{4(-1+k^2)L_{\mathrm{RES}}^4\omega_0^4}{\left(R_{\mathrm{IN(RECT)}}^2 - 2L_{\mathrm{RES}}^2\omega_0^2\right)^2}}}{\frac{2(-1+k^2)L_{\mathrm{RES}}^2}{R_{\mathrm{IN(RECT)}}^2 - 2L_{\mathrm{RES}}^2\omega_0^2}}}. \tag{13}$$

where ω_{LOW}, ω_{CENTER}, and ω_{HIGH} are a low value of ω, an intermediate value of ω corresponding to ω_0, and a high value of ω with $\mathrm{Im}[Z_{\mathrm{IN}}] = 0$, respectively. Equations (11) and (13) are only valid when k satisfies

$$k > \frac{1}{2}\sqrt{\frac{-R_{\mathrm{IN(RECT)}}^4 + 4L_{\mathrm{RES}}^2R_{\mathrm{IN(RECT)}}^2\omega_0^2}{L_{\mathrm{RES}}^4\omega_0^4}}. \tag{14}$$

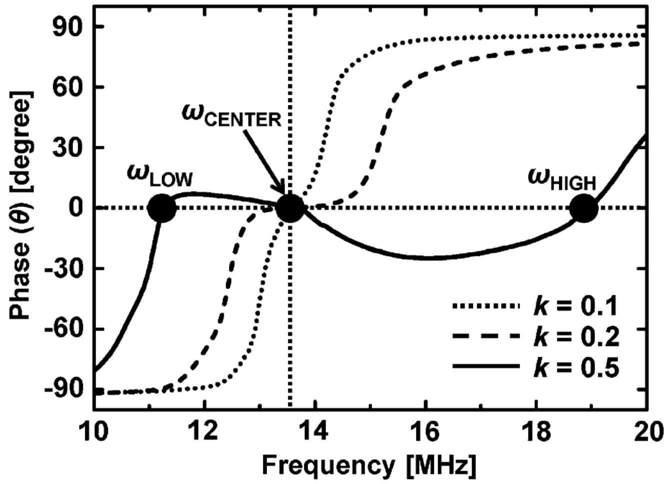

Fig. 4. Simulated frequency dependences of phase between V_{IN} and I_{IN} for $k = 0.1$, 0.2, and 0.5 with the parameters in Table I. The simulation includes a power amplifier, coupled resonators, and a rectifier. Black dots show ω_{LOW}, ω_{CENTER}, and ω_{HIGH} given by (11)–(13) for $k = 0.5$. V_{IN} and I_{IN} are defined as shown in Fig. 1(b) and are equivalent to the output voltage and output current of the power amplifier, respectively. The phase is defined as the delay of I_{IN} relative to V_{IN} at ω_0; ω at $\mathrm{Im}[Z_{\mathrm{IN}}] = 0$ and $\theta = 0$ are equivalent because the frequency dependence of $\mathrm{Im}[Z_{\mathrm{IN}}]$ corresponds approximately to that of θ.

This means that there are three solutions ($\omega = \omega_{\mathrm{LOW}}$, ω_{CENTER}, and ω_{HIGH}) satisfying $\mathrm{Im}[Z_{\mathrm{IN}}] = 0$ when the transmission distance is short, while there is only one solution ($\omega = \omega_{\mathrm{CENTER}}$) when the transmission distance is long.

Fig. 4 shows the simulated frequency dependences of the phase (θ) between the input voltage (V_{IN}) and input current (I_{IN}) to the coupled resonators in Fig. 1(b). The simulated frequency dependences of θ demonstrate that $\theta = 0$ only at $\omega = \omega_0 (= \omega_{\mathrm{CENTER}})$ when $k = 0.1$ and 0.2, while $\theta = 0$ at $\omega = \omega_0$, ω_{LOW}, and ω_{HIGH} when $k = 0.5$. This verifies the results of analysis using (11)–(14).

To increase P_2 and η_{PA}, a smaller $\mathrm{Re}[Z_{\mathrm{IN}}]$ with $\theta = 0$ should be used when the transmission distance is short. The expressions for $\mathrm{Re}[Z_{\mathrm{IN}}]$ at $\omega = \omega_{\mathrm{LOW}}$, ω_{CENTER}, and ω_{HIGH} are given by

$$\mathrm{Re}\left[Z_{\mathrm{IN}}(\omega_{\mathrm{LOW}})\right] = \mathrm{Re}\left[Z_{\mathrm{IN}}(\omega_{\mathrm{HIGH}})\right] = R_{\mathrm{IN(RECT)}} \tag{15}$$

$$\mathrm{Re}\left[Z_{\mathrm{IN}}(\omega_{\mathrm{CENTER}})\right] = \frac{k^2 L_{\mathrm{RES}}^2 \omega_0^2}{R_{\mathrm{IN(RECT)}}}. \tag{16}$$

Then, the relationships among $\mathrm{Re}[Z_{\mathrm{IN}}]$ at $\omega = \omega_{\mathrm{LOW}}$, ω_{CENTER}, and ω_{HIGH} are given by

$$\mathrm{Re}\left[Z_{\mathrm{IN}}(\omega_{\mathrm{LOW}})\right] = \mathrm{Re}\left[Z_{\mathrm{IN}}(\omega_{\mathrm{HIGH}})\right] < \mathrm{Re}\left[Z_{\mathrm{IN}}(\omega_{\mathrm{CENTER}})\right]. \tag{17}$$

Equation (17) indicates that P_2 and η_{PA} at $\omega = \omega_{\mathrm{LOW}}$ and ω_{HIGH} are larger than those at $\omega = \omega_{\mathrm{CENTER}}$ because $\mathrm{Re}[Z_{\mathrm{IN}}]$ at $\omega = \omega_{\mathrm{LOW}}$ and ω_{HIGH} is smaller than that at $\omega = \omega_{\mathrm{CENTER}}$ when the transmission distance is short. It should be noted that P_2 and η_{PA} at $\omega = \omega_{\mathrm{LOW}}$ are higher than those at $\omega = \omega_{\mathrm{HIGH}}$ because the power dissipation induced by switching loss and R_{RES} due to the skin effect increase in proportion to the frequency.

Fig. 5 shows the simulated frequency dependences of η_{PA}. When $k = 0.1$ and 0.2, η_{PA} is maximized at $\omega = \omega_{\mathrm{CENTER}}$, while η_{PA} is maximized at $\omega = \omega_{\mathrm{LOW}}$ and ω_{HIGH} when $k = 0.5$. ω with the maximum η_{PA} at each distance in Fig. 5 corresponds to the points satisfying $\theta = 0$ at $\Delta\theta/\Delta\omega > 0$ in Fig. 4. This means that ω should be controlled under the condition $\theta = 0$ at $\Delta\theta/\Delta\omega > 0$ depending on the transmission distance in order to maximize η_{PA}. Using this modified ω, η_{PA} is maximized even with the frequency splitting of η_{PA} when the transmission distance is short.

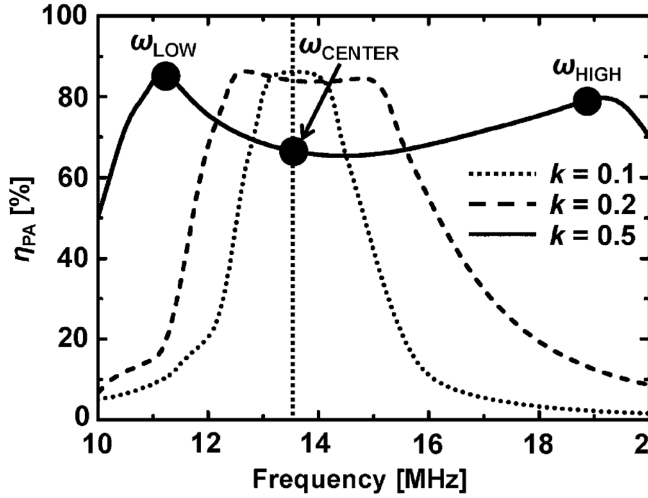

Fig. 5. Simulated frequency dependences of η_{PA} for $k = 0.1$, 0.2, and 0.5 with the parameters in Table I. The simulation includes a power amplifier, coupled resonators, and a rectifier. Black dots show ω_{LOW}, ω_{CENTER}, and ω_{HIGH} given by eqs. (11)–(13) for $k = 0.5$.

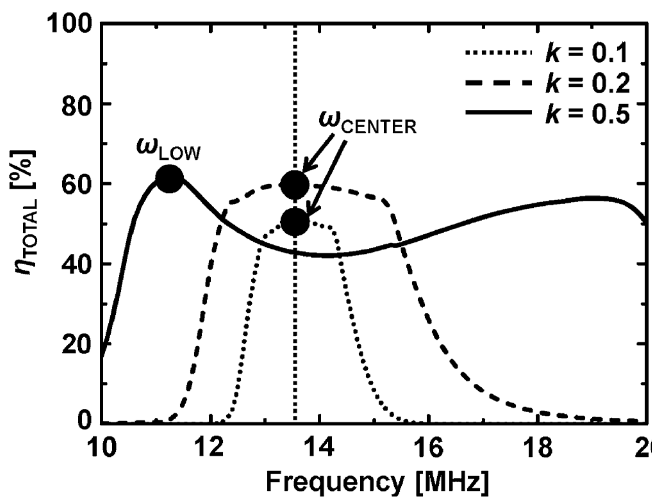

Fig. 6. Simulated frequency dependences of η_{TOTAL} for $k = 0.1$, 0.2, and 0.5 with the parameters in Table I. The simulation includes a power amplifier, coupled resonators, and a rectifier. Black dots show ω for the maximum η_{TOTAL} at each k.

C. Frequency Dependences of η_{RECT} *and* η_{TOTAL}

η_{RECT} increases proportionally to P_3 which corresponds to the output power of the power amplifier; therefore, the frequency dependences of η_{RECT} correspond approximately to that of η_{PA}.

Fig. 6 shows the simulated frequency dependences of η_{TOTAL}. Since η_{TOTAL} is the product of η_{PA}, η_{RES}, and η_{RECT}, η_{TOTAL} also exhibits frequency splitting when the transmission distance is short. The maximum efficiency is achieved at $\omega = \omega_{\mathrm{CENTER}}$ when $k = 0.1$ and 0.2, while η_{TOTAL} is maximized at $\omega = \omega_{\mathrm{LOW}}$ when $k = 0.5$.

III. Zero-Phase-Difference Capacitance Control

The origin of the frequency splitting of η_{TOTAL} in a wireless power transfer system was explained in the previous section. However, adaptive frequency control ($\theta = 0$ at $\Delta\theta/\Delta\omega > 0$) is not permitted in many radio bands. In this study, the lower peak of η_{TOTAL} is moved from ω_{LOW} to a fixed target frequency ($\omega_{\mathrm{TARGET}} = 13.56$ MHz) by changing C_{RES} in order to increase η_{TOTAL} at short distances for the fixed frequency of 13.56 MHz. Conventional studies [15]–[18] on capacitance control require bulky and expensive detectors because these algorithms for capacitance control must detect S_{11} [15] or Z_{IN} [16], [17]. On the other hand, the proposed algorithm of zero-phase-difference capacitance control (ZPDCC) only requires the phase (θ) between V_{IN} and I_{IN} for the coupled resonators in Fig. 1(b). This means that the proposed ZPDCC achieves efficient implementation in a small space using a current monitor, which is easily implemented into integrated circuits.

The duality between the capacitance dependence and the frequency dependence is given by substituting

$$\omega_0 = \frac{1}{\sqrt{L_{\mathrm{RES}} C_{\mathrm{RES}}}} \tag{18}$$

in (8)–(17). In particular, capacitance splitting corresponding to $\theta = 0$ at a fixed frequency ($\omega_{\mathrm{TARGET}} = 13.56$ MHz) is observed at

$$C_{\mathrm{LOW}} = \frac{L_{\mathrm{RES}} - \sqrt{k^2 L_{\mathrm{RES}}^2 - \frac{R_{\mathrm{L}}^2}{\omega_{\mathrm{TARGET}}^2}}}{R_{\mathrm{L}}^2 + L_{\mathrm{RES}}^2 \omega_{\mathrm{TARGET}}^2 (1-k^2)}, \tag{19}$$

$$C_{\mathrm{CENTER}} = \frac{1}{L_{\mathrm{RES}} \omega_{\mathrm{TARGET}}^2}, \tag{20}$$

$$C_{\mathrm{HIGH}} = \frac{L_{\mathrm{RES}} + \sqrt{k^2 L_{\mathrm{RES}}^2 - \frac{R_{\mathrm{L}}^2}{\omega_{\mathrm{TARGET}}^2}}}{R_{\mathrm{L}}^2 + L_{\mathrm{RES}}^2 \omega_{\mathrm{TARGET}}^2 (1-k^2)}. \tag{21}$$

Fig. 7 shows simulated capacitance dependences of the phase (θ) between V_{IN} and I_{IN} for the coupled resonators in Fig. 1(b). Similarly to the previous section, η_{TOTAL} is maximized at $C_{\mathrm{RES}} = C_{\mathrm{LOW}}$ and C_{HIGH} with capacitance splitting when the transmission distance is short, while it is maximized at $C_{\mathrm{RES}} = C_{\mathrm{CENTER}}$ at longer distances. In ZPDCC, the appropriate C_{RES} is searched for under the condition $\theta = 0$ at $\Delta\theta/\Delta C > 0$. This condition determines whether the transmission distance is short or long.

Fig. 8 shows a flow chart of the proposed algorithm for ZPDCC. To compensate for the offset of θ caused by parasitic capacitances and the delay of the current monitor, this algorithm requires calibrations of the capacitance before and after shipment. Details of the proposed algorithm are given below.

A) Calibrations before shipment
1) To compensate for parasitic capacitance and inductance on the PCB and mismatches in fabrication, the $C_{\mathrm{RES}}[\mathrm{i}]$ corresponding to the maximum η_{TOTAL} is searched for by the hill climbing method when the transmission distance is sufficiently long.
2) The obtained $C_{\mathrm{RES}}[\mathrm{i}]$ is assigned as the initial value of C_{RESINIT}. C_{RESINIT} results in the maximum η_{TOTAL} at ω_{TARGET} when the capacitance splitting of η_{TOTAL} is not observed.

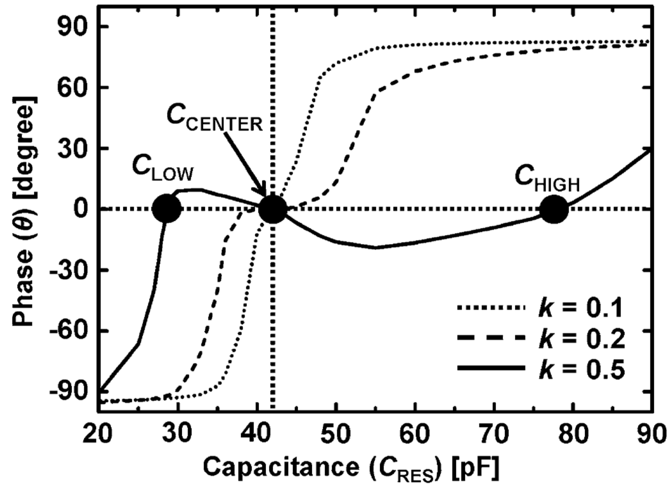

Fig. 7. Simulated capacitance dependences of phase between V_{IN} and I_{IN} at $\omega_{\mathrm{TARGET}} = 13.56$ MHz for $k = 0.1$, 0.2, and 0.5 with the parameters in Table I excluding C_{RES}. The simulation includes a power amplifier, coupled resonators, and a rectifier. Black dots show C_{LOW}, C_{CENTER}, and C_{HIGH} given by (19)–(21) for $k = 0.5$.

B) Calibrations after shipment
3) θ is measured at the calibrated C_{RESINIT} and the measured θ is assigned as the initial value of θ_{INIT}. In the proposed ZPDCC, the difference between θ and θ_{INIT} is used to discriminate whether the transmission distance is short or large. In ZPDCC, the lower peak is searched for because fewer capacitor banks are required than for a search for the higher peak. Therefore, the capacitance is finally reduced from i to i-1.
4) θ is measured at the reduced C_{RES} corresponding to i-1 and the measured θ is compared with θ_{INIT}.
5) When the measured θ is smaller than θ_{INIT}, the condition $\theta = 0$ at $\Delta\theta/\Delta C > 0$ is satisfied in ZPDCC without capacitance splitting. This means that the transmission distance is large and that C_{RESINIT} should be used as the modified C_{RES} (C_{RESMOD}).
6) When the measured θ is larger than θ_{INIT}, the transmission distance is short and capacitance splitting is observed. Therefore, C_{RESMOD} should be searched for and set to C_{LOW}. In this process, θ is repeatedly measured and compared while reducing C_{RES} until the condition $\theta \leq \theta_{\mathrm{INIT}}$ is satisfied.
7) When the measured θ is equal to θ_{INIT}, C_{RES} corresponds to C_{LOW}; therefore, C_{RES} is assigned to C_{RESMOD}.
8) When the measured θ is less than θ_{INIT}, the resolution of the capacitor bank is larger than the resolution of the phase detector. To prevent the over tune of C_{RES}, $C_{\mathrm{RES}}[\mathrm{i}+1]$ is assigned to C_{RESMOD}.

Fig. 9 shows simulated capacitance dependences of η_{TOTAL} for $k = 0.1$, 0.2, and 0.5. Capacitance splitting is only observed for $k = 0.5$. Using the proposed ZPDCC, C_{RES} is determined so that the maximum η_{TOTAL} is achieved, which depends on the transmission distance. When $k = 0.1$ and 0.2, $\theta = 0$ only at C_{CENTER}, then, using the proposed ZPDCC, it is found that $C_{\mathrm{RESMOD}} = C_{\mathrm{RESINIT}} = C_{\mathrm{CENTER}}$ as shown in Fig. 8 (case 5). On the other hand, $\theta = 0$ at C_{LOW}, C_{CENTER}, and C_{HIGH} when $k = 0.5$, then, using the proposed ZPDCC, it is found

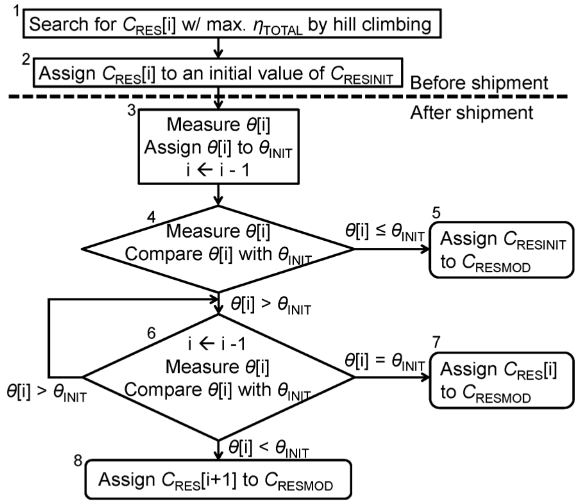

Fig. 8. Flow chart of algorithm of ZPDCC. C_{RESMOD} denotes C_{RES} modified by ZPDCC. In this algorithm, it is assumed that C_{RES} is digitally controlled. The digital code of C_{RES} is given by the integer value i.

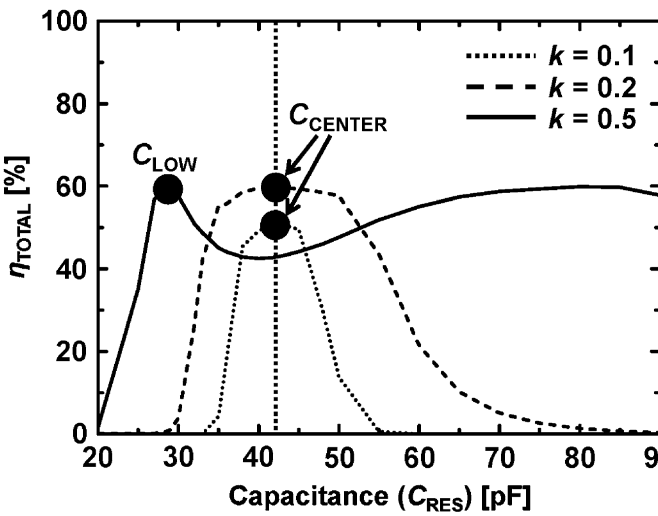

Fig. 9. Simulated capacitance dependences of η_{TOTAL} for $k = 0.1$, 0.2, and 0.5 with the parameters in Table I excluding C_{RES}. The simulation includes a power amplifier, coupled resonators, and a rectifier. Black dots show C_{RESMOD} corresponding to the maximum η_{TOTAL} for each k, which is determined by ZPDCC.

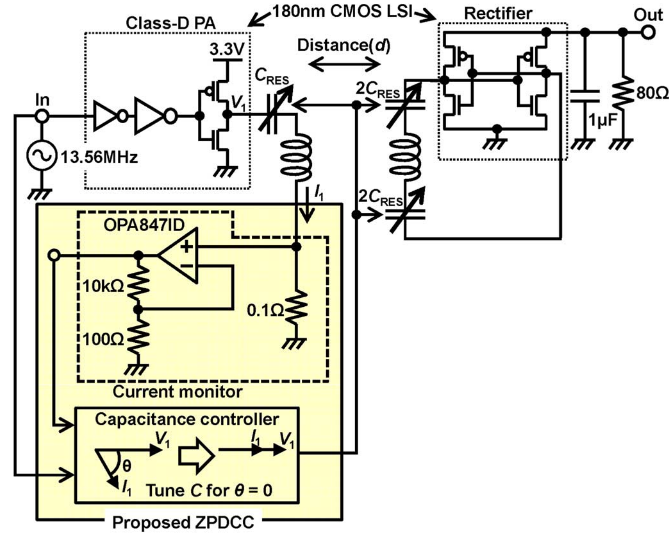

Fig. 10. Circuit schematic of wireless power transfer system in magnetic resonance with ZPDCC. All the simulation results in this paper are shown on this schematic.

that $C_{\mathrm{RESMOD}} = C_{\mathrm{LOW}}$ as shown in Fig. 8 (case 7 or 8). The modified C_{RESMOD} gives the maximum η_{TOTAL} for each k as shown in Fig. 9.

IV. Measurement Results and Discussion

To demonstrate the improvement of η_{TOTAL} upon using the proposed ZPDCC, a wireless power transfer system in magnetic resonance with the ZPDCC is implemented. Fig. 10 shows a circuit schematic of the wireless power transfer system in magnetic resonance with the ZPDCC. The class-D PA in the transmitter and the rectifier in the receiver are designed and fabricated in a 3.3 V, 180 nm CMOS process. The L_{RES} are fabricated on an FR4 PCB and the layout of the L_{RES} is the same as that in [10]. The capacitors on the PCB are implemented by ceramic capacitors.

In the circuit implementation of ZPDCC, θ is measured as the phase difference between the voltage (V_1) and current (I_1) in the transmitter. I_1 is converted to a voltage by a non-inverting amplifier, which is implemented using an operational amplifier (OPA847ID [26]) and two resistors. The gain of the amplifier is set to $1 + (10\ \mathrm{k}\Omega/100\ \Omega) = 40$ dB. In the measurement, the phase difference θ between V_1 and I_1 is measured by an oscilloscope, and the capacitance is changed by manually replacing the ceramic capacitors with a minimum resolution of 0.5 pF. The capacitance is tuned in accordance with the flow chart in Fig. 8.

To achieve automated control, the implementation of a phase detector, capacitance controller, and communication link between the transmitter and receiver is required for the integration of LSIs. First, the phase detector could be implemented in the LSIs using a time-to-digital converter (TDC) with a resolution of 20 ps ($\approx 0.1^\circ$ at 13.56 MHz) and 290 pJ/conversion-step [27]. The digitized phase data from the TDC is input to the capacitance controller (= state machine corresponding to the algorithm of ZPDCC), and the capacitance controller controls the 7-bit binary capacitor bank. The capacitor bank could be tuned by relays [15], [28] in the range of 15–45 pF on the transmitter and 30–90 pF on the receiver with a minimum resolution of 0.5 pF. In high-power applications, the on-resistance of the switches reduces η_{TOTAL} if V_{DD} is not scaled in accordance with the transmission power. The large current flow in the switches consumes a huge amount of power. On the other hand, the power consumption in the switches is not increased if V_{DD} is increased using high-voltage technologies (e.g., LDMOS and IGBT) depending on the transmission power. Such high-voltage technologies would realize highly efficient implementation with capacitance control even in high-power applications. Additionally, the on-resistance of the switches ($\approx 0.2\ \Omega$ [28]) is smaller than $R_{\mathrm{RES}}(\approx 3\ \Omega)$. This implies that the loss due to the on-resistance is not dominant in the whole system. Finally, the communication link between the transmitter and receiver could be implemented by backscattering [29], [30]. Wireless communication at 6.78 Mbps [30] without any extra antennas has been reported. The capacitor bank on the receiver is controlled in accordance with the received data. This whole system, which includes a current monitor, phase detector, capacitance controller, and communication link, is easily implemented into integrated circuits. Compared with conventional capacitance control methods

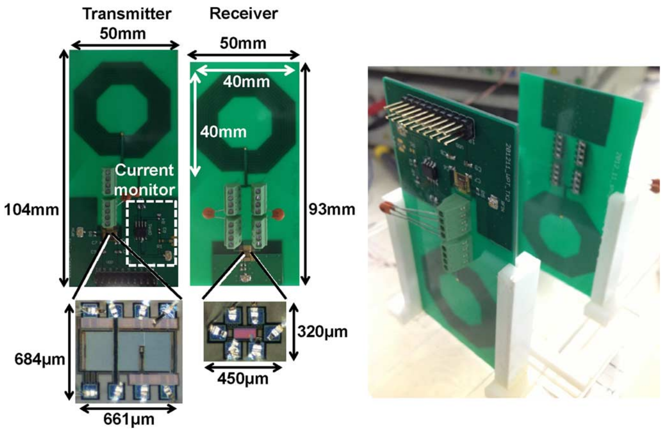

Fig. 11. Photographs of transmitter and receiver on PCB, LSIs of PA and rectifier, and measurement equipment.

TABLE II
L_{RES}, R_{RES}, AND Q FACTOR OF L_{RES} OBTAINED BY EM SIMULATION AND MEASUREMENT

	L_{RES} [µH]	R_{RES} [Ω]	Q factor
EM Simulation	3.38	2.90	96
Measurement	3.42	2.67	109

using a directional coupler [15] and a vector network analyzer [16], [17], ZPDCC is more suitable for the integration in LSIs.

Fig. 11 shows photographs of the transmitter and receiver in the wireless power transfer system in magnetic resonance. The LSIs of the PA and rectifier, and the measurement equipment are also shown in Fig. 11. The size of the L_{RES} fabricated on the PCB in the transmitter and receiver is 40 mm $\times$ 40 mm. The core sizes of the PA and rectifier are 684 μm $\times$ 661 μm and 320 μm $\times$ 450 μm, respectively.

Table II shows a comparison of L_{RES}, R_{RES}, and the Q factor of the L_{RES} obtained by EM simulation and measurement at 13.56 MHz. The measurement results are in good agreement with the values in Table I. This means that the simulated results in previous sections and the measurement results are consistent.

Fig. 12 shows a comparison of $|S_{21}|$ for coupled resonators at transmission distances (d) of 5 mm, 15 mm, and 25 mm obtained by EM simulation and measurement. The measurement results are consistent with the simulated results and frequency splitting at $d = 5$ mm is observed.

Fig. 13 shows the simulated transmission distance dependence of the coupling coefficient (k) at 13.56 MHz. This result shows that the parameters ($k = 0.1,\ 0.2,$ and 0.5) used in previous sections approximately correspond to $d = 5$ mm, 15 mm, and 25 mm, respectively.

Fig. 14 shows the measured frequency dependences of η_{TOTAL} at $d = 5$ mm, 15 mm, and 25 mm. When $d = 15$ mm and 25 mm, the frequency dependences of η_{TOTAL} do not exhibit frequency splitting; therefore, η_{TOTAL} is maximized at 13.56 MHz. In contrast, the frequency dependence of η_{TOTAL} at $d = 5$ mm exhibits frequency splitting. η_{TOTAL} at $d = 5$ mm is maximized at the lower peak corresponding to ω_{LOW}.

Fig. 15 shows the measured capacitance dependences of θ at 13.56 MHz when $d = 5$ mm, 15 mm, and 25 mm. When $d = 15$ mm and 25 mm, $\theta = 0$ once, which corresponds to $C_{\mathrm{CENTER}} (= 37\ \mathrm{pF})$ with the maximum η_{TOTAL}. In contrast,

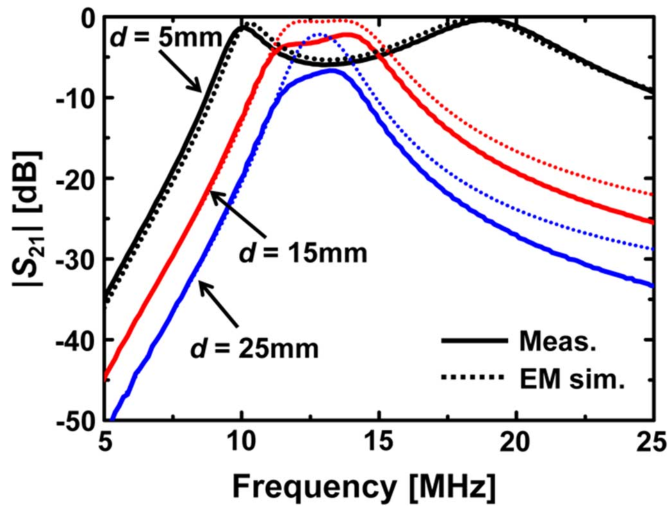

Fig. 12. EM-simulated and measured frequency dependences of $|S_{21}|$ in coupled resonators at transmission distances (d) of 5 mm, 15 mm, and 25 mm.

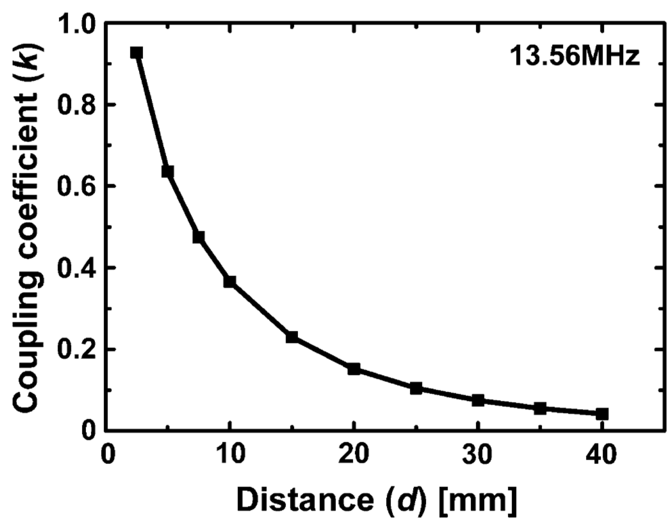

Fig. 13. Simulated transmission distance dependence of coupling coefficient (k) at 13.56 MHz.

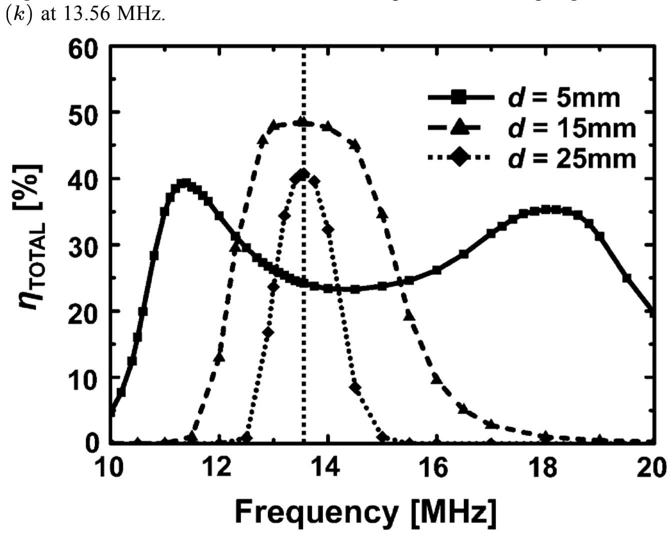

Fig. 14. Measured frequency dependences of η_{TOTAL} at $C_{\mathrm{RES}} = 37$ pF when $d = 5$ mm, 15 mm, and 25 mm.

when $d = 5$ mm, $\theta = 0$ at C_{LOW} and C_{CENTER}. C_{RES} is modified from $C_{\mathrm{CENTER}} (= 37\ \mathrm{pF})$ to $C_{\mathrm{LOW}} (= 25\ \mathrm{pF})$ by the proposed ZPDCC with the condition $\theta = 0$ at $\Delta\theta/\Delta C > 0$

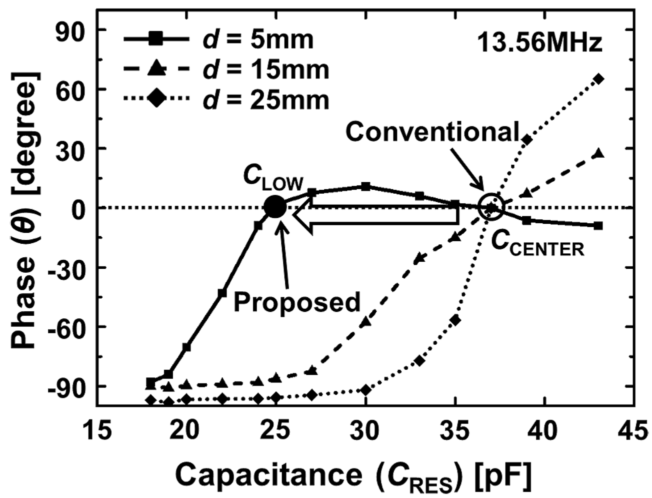

Fig. 15. Measured capacitance dependences of θ at 13.56 MHz when $d = 5$ mm, 15 mm, and 25 mm. θ is measured by an oscilloscope.

when the transmission distance is short $(d = 5\ \mathrm{mm})$. The relay switches should have an operation time of 1 ms [28] to 5 ms [15] and be the slowest block in the automated ZPDCC. The maximum iteration step is determined at the minimum transmission distance. At the minimum distance of 2.5 mm, the capacitor is tuned from 37 pF to 20 pF with a minimum step of 0.5 pF. This corresponds to 35 steps and a settling time of less than 200 ms.

Fig. 16 shows the measured capacitance dependences of η_{TOTAL} at 13.56 MHz when $d = 5$ mm, 15 mm, and 25 mm. When $d = 15$ mm and 25 mm, η_{TOTAL} is maximized at C_{CENTER} of 37 pF. In contrast, η_{TOTAL} at $d = 5$ mm is maximized at C_{LOW} of 25 pF. Using the proposed ZPDCC, η_{TOTAL} is increased from 25% to 34% with the capacitance control of C_{RES} from $C_{\mathrm{CENTER}}(= 37\ \mathrm{pF})$ to $C_{\mathrm{LOW}}(= 25\ \mathrm{pF})$. The measured load power (P_4) at $d = 5$ mm is also increased from 4.8 mW to 8.4 mW. The maximum P_4 of 56 mW is achieved at $d = 30$ mm. On the other hand, the measured η_{TOTAL} at $d = 5$ mm is lower than the simulated η_{TOTAL} owing to the coarse minimum resolution of $C_{\mathrm{RES}}(= 0.5\ \mathrm{pF})$ and the mismatches of C_{RES} between the transmitter and receiver. η_{TOTAL} at short distances will be increased if the fine minimum resolution of C_{RES} and a calibration method between the transmitter and receiver are realized.

Fig. 17 shows the measured transmission distance (d) dependence of η_{TOTAL} at 13.56 MHz. The conventional constant capacitance method and the proposed ZPDCC are compared. When d is longer than 10 mm, ZPDCC does not modify C_{RES} from C_{CENTER}. Therefore, η_{TOTAL} for the proposed ZPDCC and the conventional constant capacitance method would be equivalent under ideal conditions. In the measurement, however, η_{TOTAL} for ZPDCC is 1–7% lower than that for the conventional constant capacitance method because of the resistive loss of 0.1 Ω for the current monitor shown in Fig. 10. In contrast, when d is less than 10 mm, η_{TOTAL} for ZPDCC is higher than that for the conventional constant capacitance method, which indicates that the increase in η_{TOTAL} caused by ZPDCC exceeds the decrease in η_{TOTAL} caused by the resistive loss. For example, η_{TOTAL} increases 1.7-times from 16% to 27% at $d = 2.5$ mm upon tuning C_{RES} from 37 pF to 20 pF. In ZPDCC, the maximum η_{TOTAL} is 49% at $d = 15$ mm.

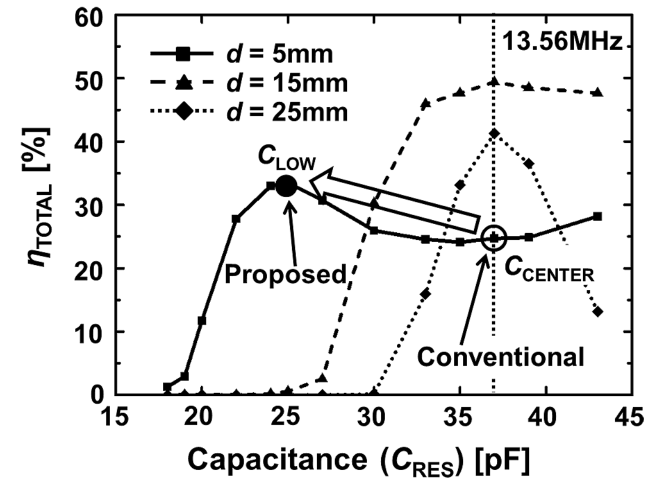

Fig. 16. Measured capacitance dependences of η_{TOTAL} at 13.56 MHz when $d = 5$ mm, 15 mm, and 25 mm.

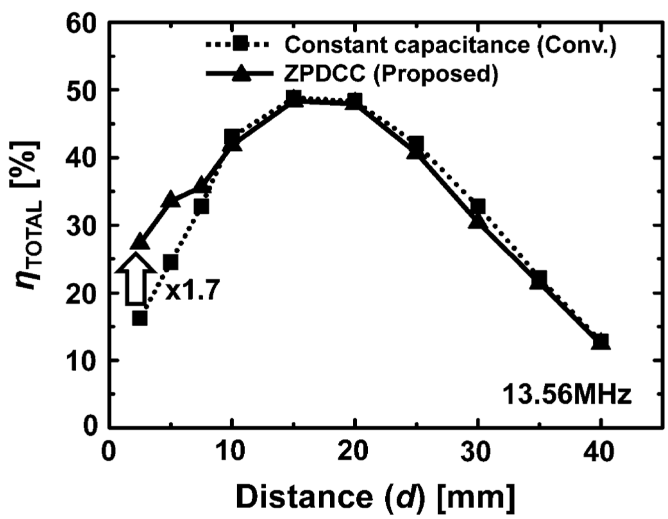

Fig. 17. Measured distance dependences of η_{TOTAL} using conventional constant capacitance method and proposed ZPDCC at 13.56 MHz.

Table III shows a comparison with the results for previously reported wireless power transfer systems at a fixed frequency. At a fixed frequency, only V_{DD} control [13] and impedance matching [15] target the efficiency degradation. This work is the first report of capacitance control including a power amplifier and a rectifier; additionally, the directional coupler used in the previous impedance-matching method is not required. The V_{DD} control method does not include the loss of the DC-DC converter. The efficiency of the corresponding state-of-the-art DC-DC converter is 60–85% in the voltage range 0.6–2.5 V [31]. This implies that the efficiency of the previous V_{DD} control method is greatly reduced by the low efficiency of the DC-DC converter.

V. Conclusion

In this paper, zero-phase-difference capacitance control (ZPDCC), which is suitable for integration in LSIs was proposed to solve the problem of efficiency degradation of the magnetic resonance at short distances. The proposed ZPDCC achieves adaptive capacitance control by a newly proposed control algorithm in which $\theta = 0$ at $\Delta\theta/\Delta C > 0$ with a current-sensing circuit to control variable capacitors at a fixed

TABLE III
COMPARISON WITH RESULTS FOR PREVIOUSLY REPORTED WIRELESS POWER TRANSFER SYSTEMS AT FIXED FREQUENCY

	Control method	Frequency	TX-RX coil diameter	R_L	Max. η_{TOTAL}	Distance at max. η_{TOTAL}	Load Power at max. η_{TOTAL}
[13]	V_{DD} control	6.785MHz	30-30mm	10kΩ	†74%	2mm	10mW
[15]	Impedance matching	13.56MHz	300-300mm	50Ω	‡85%	150mm	6.8W
This work	ZPDCC	13.56MHz	40-40mm	80Ω	49%	15mm	24mW

†DC-DC converter is not included. ‡PA and rectifier are not included.

†DC-DC converter is not included. ‡PA and rectifier are not included.

frequency. Additionally, a theoretical analysis of η_{TOTAL} including a power amplifier, coupled resonators, and a rectifier was demonstrated in this paper. A wireless power transfer system in magnetic resonance with ZPDCC is fabricated in a 3.3 V, 180 nm CMOS. By introducing ZPDCC, the measured η_{TOTAL} at an f_{RES} of 13.56 MHz increases 1.7-times from 16% to 27% at $d = 2.5$ mm.

ACKNOWLEDGMENT

The authors thank Masayuki Mizuno, Koichi Yamaguchi, Haruya Ishizaki, Hideki Sasaki, Tatsuaki Tsukuda, Hiroki Sugimoto, Yuji Shinohara, and Tomotoshi Nureki of Renesas Electronics Corporation for encouragement and discussions.

The VLSI chips in this study were fabricated as part of the chip fabrication program of VLSI Design and Education Center (VDEC), the University of Tokyo, in collaboration with Rohm Corporation and Toppan Printing Corporation.

The author Shunta Iguchi is supported by Japan Society for the Promotion of Science through the Program for Leading Graduate Schools (MERIT).

REFERENCES

[1] A. Kurs, A. Karalis, R. Moffatt, J. D. Joannopoulos, P. Fisher, and M. Soljacic, "Wireless power transfer via strongly coupled magnetic resonances," *Science*, vol. 317, pp. 83–86, Jul. 2007.

[2] W. C. Brown, "Experiments in the transportation of energy by microwave beam," in *Proc. IRE Int. Convention Rec.*, Mar. 1964, vol. 12, pp. 8–17.

[3] G. Jong and B. Cho, "An energy transmission system for an artificial heart using leakage inductance compensation of transcutaneous transformer," *IEEE Trans.Power Electron.*, vol. 13, no. 6, pp. 1013–1022, Nov. 1998.

[4] A. P. Sample, D. A. Meyer, and J. R. Smith, "Analysis, experimental results, range adaptation of magnetically coupled resonators for wireless power transfer," *IEEE Trans. Ind. Electron.*, vol. 58, no. 2, pp. 544–554, Feb. 2011.

[5] D. Ahn and S. Hong, "A transmitter or a receiver consisting of two strongly coupled resonators for enhanced resonant coupling in wireless power transfer," *IEEE Trans. Ind. Electron.*, vol. 61, no. 3, pp. 1193–1203, Mar. 2014.

[6] D. Ahn and S. Hong, "Wireless power transmission with self-regulated output voltage for biomedical implant," *IEEE Trans. Ind. Electron.*, vol. 61, no. 5, pp. 2225–2235, May 2014.

[7] J. Park, Y. Tak, T. Kim, Y. Kim, and S. Nam, "Investigation of adaptive matching methods for near-field wireless power transfer," *IEEE Trans. Antennas Propag.*, vol. 59, no. 5, pp. 1769–1773, May 2011.

[8] Q. Chen, S. C. Wong, C. K. Tse, and X. Ruan, "Analysis, design, control of a transcutaneous power regulator for artificial hearts," *IEEE Trans. Biomed. Circuits Syst.*, vol. 3, no. 1, pp. 23–31, Feb. 2009.

[9] A. J. Moradewicz and P. Kazmierkowski, "Contactless energy transfer system with FPGA-controlled resonant converter," *IEEE Trans. Ind. Electron.*, vol. 57, no. 9, pp. 3181–3190, Sep. 2010.

[10] K. Mori, H. Lim, S. Iguchi, K. Ishida, M. Takamiya, and T. Sakurai, "Positioning-free resonant wireless power transmission sheet with staggered repeater coil array (SRCA)," *IEEE Antennas Wireless Propag. Lett.*, vol. 11, pp. 1710–1713, 2012.

[11] Y. Narusue, Y. Kawahara, and T. Asami, "Impedance matching method for any-hop straight wireless power transmission using magnetic resonance," in *Proc. IEEE RWS*, Jan. 2013, pp. 20–23.

[12] G. Wang, W. Liu, M. Sivaprakasam, and G. A. Kendir, "Design and analysis of an adaptive transcutaneous power telemetry for biomedical implants," *IEEE Trans. Circuits Syst. I, Reg. Papers*, vol. 52, no. 10, pp. 2109–2117, Oct. 2005.

[13] M. W. Baker and R. Sarpeshkar, "Feedback analysis and design of RF power links for low-power bionic system," *IEEE Trans. Biomed. Circuits Syst.*, vol. 1, no. 1, pp. 28–38, Mar. 2007.

[14] Y. Moriwaki, T. Imura, and Y. Hori, "Basic study on reduciton of reflected power using DC/DC converters in wireless power transfer system via magnetic resonant coupling," in *Proc. IEEE INTELEC*, Oct. 2011, pp. 1–5.

[15] T. C. Beh, M. Kato, T. Imura, S. Oh, and Y. Hori, "Automated impedance matching system for robust wireless power transfer via magnetic resonance coupling," *IEEE Trans. Ind. Electron.*, vol. 60, no. 9, pp. 3689–3698, Sep. 2013.

[16] K. Sasaki, S. Sugiura, and H. Iizuka, "Distance adaptation method for magnetic resonance coupling between variable capacitor-loaded parallel-wire coils," *IEEE Trans. Microw. Theory Tech.*, vol. 62, no. 4, pp. 892–900, Apr. 2014.

[17] K. Ogawa, N. Oodachi, S. Obayashi, and H. Shoki, "A study of efficiency improvement of wireless power transfer by impedance matching," in *Proc. IEEE IMWS-IWPT*, May 2012, pp. 155–157.

[18] E. M. Thomas, J. D. Heebl, C. Pfeiffer, and A. Grbic, "A power link study of wireless non-radiative power tranfer systems using resonant shielded loops," *IEEE Trans. Circuits Syst. I, Reg. Papers*, vol. 59, no. 9, pp. 2125–2136, Sep. 2012.

[19] S. Iguchi, P. Yeon, H. Fuketa, K. Ishida, T. Sakurai, and M. Takamiya, "Zero phase difference capacitance control (ZPDCC) for magnetically resonant wireless power transmission," in *Proc. IEEE WPTC*, May 2013, pp. 25–28.

[20] J. J. Casanove, Z. N. Low, and J. Lin, "Design and optimization of a class-E amplifier for a loosely coupled planar wireless power system," *IEEE Trans. Circuits Syst. II, Exp. Briefs*, vol. 56, no. 11, pp. 830–834, Nov. 2009.

[21] I. Awai and T. Ishizaki, "Transferred power and efficiency of a coupled-resonator WPT system," in *Proc. IEEE IMWS-IWPT*, May 2012, pp. 105–108.

[22] J. L. Villa, J. Sallan, J. F. S. Osorio, and A. Llombart, "High-misalignment tolerant compensation topology for ICPT systems," *IEEE Trans. Ind. Electron.*, vol. 59, no. 2, pp. 945–951, Feb. 2012.

[23] N. Inagaki, "Theory of image impedance matching for inductively coupled power transfer systems," *IEEE Trans. Microw. Theory Tech.*, vol. 62, no. 4, pp. 901–908, Apr. 2014.

[24] "Frequency allocations of amateur satellite service," Article 5, 5.150, ISM applications, ITU [Online]. Available: http://www.itu.int/en/ITU-R/space/AmateurDoc/ARS-ART5_E.pdf

[25] Virtuoso Multi-Mode Simulation With SPECTRE Platform, Spectre RF Datasheet, Cadence Design Systems, Inc. [Online]. Available: http://www.cadence.com/rl/Resources/datasheets/virtuoso_mmsim.pdf#page=4

[26] Wideband, Ultra-Low Noise, Voltage Feedback Operational Amplifier, OPA847ID Datasheet, Texas Instruments [Online]. Available: http://www.ti.com/lit/ds/symlink/opa847.pdf

[27] R. B. Staszewski, S. Vemulapalli, P. Vallur, J. Wallberg, and P. T. Balsara, "1.3 V 20 ps time-to-digital converter for frequency synthesis in 90-nm CMOS," *IEEE Trans. Circuits Syst. II, Ex. Briefs*, vol. 53, no. 3, pp. 220–224, Mar. 2006.

[28] Reed relay, D31B3100 Datasheet, Celduc Relais [Online]. Available: http://www.celduc-relais.com/all/pdfcelduc/D31B_1_0.pdf

[29] X. Li, C. Tsui, and W. Ki, "A 13.56 MHz wireless power transfer system with reconfigurable resonant regulating rectifier and wireless power control for implantable medical devices," in *IEEE Symp. VLSI Circuits Dig. Tech. Papers*, Jun. 2014, pp. 28–29.

[30] S. Ha, C. Kim, J. Park, S. Joshi, and G. Cauwenberghs, "Energy-recycling integrated 6.78-Mbps data 6.3-mW power telemetry over a single 13.56 MHz inductive link," in *IEEE Symp. VLSI Circuits Dig. Tech. Papers*, Jun. 2014, pp. 66–67.

[31] L. G. Salem and P. P. Mercier, "An 85%-efficiency fully integrated 15-ratio recursive switched-capacitor DC-DC converter with 0.1-to-2.2 V output voltage range," in *IEEE Int. Solid-State Circuits Conf. Dig. Tech. Papers*, Feb. 2014, pp. 88–89.

Shunta Iguchi (S'12) received the B.S. degree in electronic engineering from the University of Electro-Communications, Tokyo, Japan, in 2011 and the M.S. degree in electrical engineering and information systems, from the University of Tokyo, Tokyo, in 2013, where he is currently pursuing a Ph.D. degree. His research interests include the design of low-power RF transceiver circuits, crystal oscillators, and wireless power transmission circuits.

From August 2011 to September 2011, he worked at Analog Devices, Tokyo. From August 2013 to September 2013, he worked at Toshiba, Kawasaki, Japan. From August 2014 to October 2014, he worked at TSMC, Hsinchu, Taiwan. All of his industrial experience was as an intern. He is a recipient of the best paper award at the 2013 IEEE Wireless Power Transfer Conference.

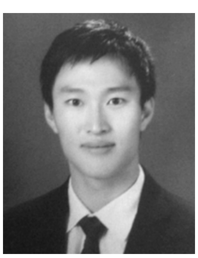

Pyungwoo Yeon (S'14) received the B.Sc. degree in electrical and computer engineering from Seoul National University, Seoul, Korea, in 2010, and the M.S. degree in electrical engineering and information systems from the University of Tokyo, Tokyo, Japan, in 2012. He is now pursuing his doctoral degree in the electrical and computer engineering at Georgia Institute of Technology, Atlanta, GA, USA, and working on developing wirelessly powered implantable biomedical system at the GT-Bionics Lab.

From February 2012 to May 2014, he worked as an analog IC designer at Samsung Electronics, Yongin, Korea, designing wireless power receiver IC for mobile devices. His research interests include analog/mixed-signal integrated circuit design, wireless power/data transfer, energy harvesting, and biomedical/implantable system design.

Hiroshi Fuketa (S'07–M'10) received the B.E. degree from Kyoto University, Kyoto, Japan, and the M.E. and Ph.D. degrees in information systems engineering from Osaka University, Osaka, Japan, in 2002, 2008 and 2010, respectively.

Currently, he is a Research Associate with Institute of Industrial Science, the University of Tokyo, Tokyo, Japan. His research interests include ultra-low power circuit design and large area electronics with organic transistors. Dr. Fuketa is a member of IEICE.

Koichi Ishida (S'00–M'06) received the B.S. degree in electronics engineering from the University of Electro-Communications, Tokyo, Japan, in 1998, and received the M.S. and Ph.D. degrees in electronics engineering from the University of Tokyo, Tokyo, in 2002 and 2005, respectively.

He joined Nippon Avionics Co., Ltd. Yokohama, Japan, in 1989, where he developed high-reliability hybrid microcircuits for aerospace programs. From 2005 to 2007, he worked for CMOS analog and RF circuits at Tokyo Institute of Technology, Yokohama, Japan. From 2007 to 2012, he worked for on-chip power supply circuits and organic electronics circuits at the Institute of Industrial Science, the University of Tokyo, Tokyo. Since July 2012, he has been working at Chair for Circuit Design and Network Theory, Technische Universität Dresden, Dresden, Germany. His research interests include low-voltage low-power CMOS analog circuits, on-chip power supply circuits, and large-area flexible electronics. Dr. Ishida is a member of IEICE.

Takayasu Sakurai (S'77–M'78–SM'01–F'03) received the Ph.D. degree in EE from the University of Tokyo, Tokyo, Japan, in 1981. In 1981 he joined Toshiba Corporation, where he designed CMOS DRAM, SRAM, RISC processors, DSPs, and SoC Solutions. He has worked extensively on interconnect delay and capacitance modeling known as Sakurai model and alpha power-law MOS model. From 1988 through 1990, he was a visiting researcher at the University of California Berkeley, where he conducted research in the field of VLSI CAD. From 1996, he has been a Professor at the University of Tokyo, working on low-power high-speed VLSI, memory design, interconnects, ubiquitous electronics, organic ICs, and large-area electronics. He has published more than 600 technical publications including 100 invited presentations and several books and filed more than 200 patents.

He is the executive committee chair for VLSI Symposia and a steering committee chair for the IEEE A-SSCC. He served as a conference chair for the Symp. on VLSI Circuits, and ICICDT, a vice chair for ASPDAC, a TPC chair for the A-SSCC, and VLSI symp., an executive committee member for ISLPED and a program committee member for ISSCC, CICC, A-SSCC, DAC, ESSCIRC, ICCAD, ISLPED, and other international conferences. He is a recipient of 2010 IEEE Donald O. Pederson Award in Solid-State Circuits, 2009 and 2010 IEEE Paul Rappaport award, 2010 IEICE Electronics Society award, 2009 IEICE achievement award, 2005 IEEE ICICDT award, 2004 IEEE Takuo Sugano award, and 2005 P&I patent of the year award and four product awards. He delivered keynote speech at more than 50 conferences including ISSCC, ESSCIRC and ISLPED. He was an elected AdCom member for the IEEE Solid-State Circuits Society and an IEEE CAS and SSCS distinguished lecturer. He is also a domain research supervisor for nano-electronics area in Japan Science and Technology Agency. He is an IEICE Fellow.

Makoto Takamiya (S'98–M'00–SM'14) received the B.S., M.S., and Ph.D. degrees in electronic engineering from the University of Tokyo, Tokyo, Japan, in 1995, 1997, and 2000, respectively. In 2000, he joined NEC Corporation, Japan, where he was engaged in the circuit design of high speed digital LSIs. In 2005, he joined University of Tokyo, Japan, where he is an associate professor of VLSI Design and Education Center. From 2013 to 2014, he stayed at University of California, Berkeley, as a visiting scholar. His research interests include the circuit design of the low-power RF circuits, the ultra low-voltage logic circuits, the low-voltage power management circuits, and the large area and flexible electronics with organic transistors.

He is a member of the technical program committee of IEEE International Solid-State Circuits Conference and IEEE Symposium on VLSI Circuits. He received 2009 and 2010 IEEE Paul Rappaport Awards and the best paper award in 2013 IEEE Wireless Power Transfer Conference.